European Polymer Journal 173 (2022) 111300

Contents lists available at ScienceDirect

European Polymer Journal

journal homepage: www.elsevier.com/locate/europolj

The effect of solvent and pressure on polycaprolactone solutions for particle and fibre formation

Esra Altun [a,1], Jubair Ahmed [a,1], Mehmet Onur Aydogdu [a,1], Anthony Harker [b], Mohan Edirisinghe [a,*]

[a] Department of Mechanical Engineering, University College London, London WC1E 7JE, UK
[b] London Centre for Nanotechnology and Department of Physics & Astronomy, University College London, London WC1E 6BT, UK

ARTICLE INFO

Keywords:
PCL
Electrospraying
Pressurised gyration
Solvent
Gas pressure

ABSTRACT

Polycaprolactone (PCL) is a widely used material in many applications to tackle health problems worldwide. Formed micro- or nanosized PCL particles and fibres benefit from a higher surface area to volume ratio and are valuable in those applications, thus there is always a push to achieve smaller diameters. Electrohydrodynamic (EHD) technologies have been at the forefront in the production of polymeric biomaterials, and pressurised gyration (PG) has also enhanced possibilities by its ability to spin comparable fibres at rapid speeds. In this work, PCL microparticles and fibres were separately produced by changing key operating parameters of EHD and PG systems and PCL solution properties. Initially, PCL microparticles were formed by electrospraying with different binary solvent systems, followed by pressurised gyration fibre production with various singular solvents and a pre-optimised binary solvent system. As anticipated, the use of binary systems altered particle morphologies and diameters, while increased pressure and the use of different solvents greatly affected the characteristics of resulting fibres. The morphology of PCL was found to be highly dependent on the solvents and operating parameters of the technology used.

1. Introduction

Polycaprolactone (PCL) has been used for decades as an indispensable bioresorbable polymer having uses in a variety of drug delivery and tissue engineering applications [1–3]. It is an attractive polymer holding many advantageous properties for instance having good cytocompatibility, non-toxic properties, suitable mechanical properties and a unique degradation pattern of up to 2 years, while its prolonged drug release profile can reach beyond several months [4,5]. It has good solubility in a range of organic solvents, making it versatile in processing into a variety of materials [6–8]. Due to this excellent solubility, it has been formed into various products such as nanospheres, nanoparticles, fibres, and foams [9,10].

Various methods such as electrospraying [11], electrospinning [12], solution blow spinning [13], and centrifugal spinning [14] have been well studied in conjunction with biopolymer PCL [15]. Electrospraying, which provides control over particle morphology, is one of the most preferred methods in particle production. It can meet industrial scale requirements as the particle type and size can be tailored according to the needs of the application area and the demand of the market [16]. In fibre production, electrospinning is hindered by the limits of low yield and achieving mass production on an industrial scale. Therefore, other techniques such as solution blow spinning and centrifugal spinning have been proposed and used. Pressurised gyration, on the other hand, is a new method which can generate PCL fibres on an industrial scale, while tailoring fibre characteristics such as diameter and fibre-mesh alignment [5,17,18].

When it comes to the delivery of active ingredients such as drugs and antimicrobials for pharmaceutical applications, electrospinning has been eclipsed by electrospraying due to its products having a higher surface area to volume ratio [19]. This production mechanism works by exposing the polymer solution to a very high electrostatic force which causes the polymer solution to transform into a rapidly ejected jet from a nozzle that is then broken up and deposited randomly on an electrically grounded collector. Micro- or nanosized particles produced retain a high surface area without being limited by problems such as aggregation, due

* Corresponding author.
E-mail address: m.edirisinghe@ucl.ac.uk (M. Edirisinghe).
[1] Equal contributions.

https://doi.org/10.1016/j.eurpolymj.2022.111300
Received 2 April 2022; Received in revised form 17 May 2022; Accepted 19 May 2022
Available online 25 May 2022

to the rapid evaporation phenomenon of the system [20].

Pressurised gyration is a more recent process that uses centrifugal spinning and solution blow spinning to mass produce non-woven fibres in which the average fibre diameters range between micro- to nanometres [21]. The process involves a rapid rotation of a pot with multiple small orifices through its wall, which generates a centrifugal force on the polymer solution forming polymeric fibres, this process involves the use of an external gas pressure that helps to significantly reduce the fibre diameter [22]. The ability to control processing parameters including rotational speed and gas pressure allows for tailoring the morphology of fibres and other polymeric structures such as beads and bubbles [23,24].

The morphology of polymeric products is primarily dependent on solution properties such as viscosity, molecular weight of the polymer, surface tension, and even solution density in both electrospraying and pressurised gyration methods [25–28]. During the spraying or spinning of a polymer solution, the choice of solvent is highly influential in determining the solution properties. In pressurised gyration-based techniques, the main driving forces for fibre production are the centrifugal force exerted by the rotating pot and the gas pressure inside this vessel, so properties such as electrical conductivity and dielectric constant are not important properties [29,30]. In electrospraying, the electric field overcomes the surface tension of the fluid immediately before a jet appears [31]. With gyration techniques, centrifugal force and gas pressure work in tandem to overcome the surface tension of the polymer solution within the vessel. Therefore, surface tension and viscosity have emerged as the major properties affecting fibre morphology [32,33].

Pressure also affects the diameter of fibres spun by pressurised gyration. With a Poly(ethylene oxide) polymer system using water as its solvent, it is observed that the fibre diameter reduced with each increment of applied pressure [34]. As the polymer jet escapes the orifices of the gyration vessel, it is elongated by the motion of the centrifugal force and the momentum from its exit velocity, this causes thinning of the jet which can result in thinner fibres. Solvents of high volatility can reduce the effect of jet thinning as the jet rapidly solidifies as the solvent evaporates. For this reason, the effect of solvent and applied pressure was investigated to determine its result on product morphology and average fibre diameter. Solvents with varying volatilities, densities, and vapour pressures were used whilst keeping concentration and processing parameters constant. After the experiments, morphologies of the resulting polymeric structures were thoroughly explored.

As pressure affects the morphology of the produced polymeric products in pressurised gyration, other operating parameters during electrospraying can have differing outcomes on the particles produced. These parameters can be divided into three major categories; solution flow rate, applied voltage, and working distance; whilst environmental parameters include relative humidity and ambient temperature [35]. Moreover, these parameters play a key factor in altering the morphology of electrospraying products according to the desired outcomes and requirements for particular applications [23]. Therefore, tuning the parameters of the production phase is crucial for the production of precise functional particles.

In this study, PCL structures were produced using both electrospraying and pressurised gyration in an attempt to understand how the solvent systems and operating parameters affect the final product morphology for this polymer which helps many healthcare applications. The effect of different solvents stated in literature for making PCL particles or fibres and working parameter combinations on product morphology were thoroughly investigated. The use of PCL as the model polymer was expected to demonstrate how solvent selection, with both binary and lone solvents, will lead to remarkably different polymeric morphologies. Additionally, the importance of operating parameters and the customisability they offer in tailoring the final product morphology with multiple manufacturing technologies consisting of electrospraying and pressurised gyration has been emphasised and where possible properly connections are mentioned.

2. Materials and methods

2.1. Reagents

Polycaprolactone (PCL) pellets, Mn 14,000 (for electrospraying) and Mn 80,000 (for pressurised gyration), acetone (Ace), chloroform (Chl), dichloromethane (Dcm), dimethylformamide (Dmf), ethanol (EtOh), methanol (MeOh), tetrahydrofuran (Thf), and toluene (Tol) were purchased from Sigma-Aldrich (St. Louis, MO, USA). All reagents were of analytical grade and used as received. The properties of each solvent are summarised in Table 1. The molecular weight of the polymer along with the polymer concentration in solution has a substantial influence on rheological behaviour and properties and determines chain entanglement [36]. Preliminary experiments showed that the PCL chosen for electrospraying which has a low molecular weight is more suited for making particles and the PCL with a high molecular weight is ideal for making fibres.

During solvent selection, choosing ones that are related to PCL in the literature was the main focus. Even though during both electrospraying and pressurised gyration, all the excess solvent is evaporated, and final product is always a dry material, it is important to use polymer friendly and production method friendly solvents.

2.2. Spraying PCL particles with electrospraying

2% (w/v) PCL solutions were prepared using Chl combined with Ace, MeOh, EtOh and Dcm at three different ratios (3:1, 1:1, and 1:3 v/v) making Chl:Ace, Chl:EtOh, Chl:MeOh, and Chl:Dcm blends. Each solvent blend was stirred for 24 h using a magnetic stirrer to completely dissolve the PCL pellets.

After dissolving the PCL in solvent blends, electrospraying was carried out providing constant environmental conditions such as atmospheric pressure, 59% relative humidity, and ambient temperature of 20°C for each solution. A schematic representation of the electrospraying setup is illustrated in Fig. 1. A high voltage power supply (Glassman High Voltage Inc., NJ, United States, Fig. 1**(b)**) that is capable of applying DC voltage up to 30 kV and for negatively charging the directly connected stainless-steel nozzle (0.5 mm inner and 0.8 mm outer diameters, as shown in Fig. 1**(c)**) was used. An electric field was formed between the nozzle and grounded stainless-steel collector plate (Fig. 1**(d)**) to allow the polymeric solution to migrate from droplets to the jet and initiate particle deposition. The collection distance for each experiment was 160 mm. During the process, polymeric solution was fed into the system using a PTFE tubing (Sigma-Aldrich, St. Louis, MO, USA) and a high precision syringe pump (Harvard Apparatus Ltd., Edenbridge, UK, Fig. 1**(a)**) using a constant 2 μm/min flow rate. Voltage was set to 18 kV.

2.3. Spinning PCL fibres with pressurised gyration

PCL solutions in Ace, Chl, Dcm, Dmf, Thf, and Tol were prepared at a concentration of 15% (w/v). This concentration was chosen because it provided optimal yields in an exploratory study. The optimised binary solvent (3:1 Chl:MeOh) from the electrospraying work was also spun with pressurised gyration to draw a comparison between the binary solvent using different techniques, for this, 15% (w/v) PCL solution was used to ensure sufficient polymer chain entanglement. The solutions were stored in an airtight 50 mL glass vial where they were subjected to high-speed mixing at 3600 rpm for 20 min (Hauschild SpeedMixer DAC 150.1 FVZ-K, Germany), at 5 min intervals to ensure heat did not accumulate. Solutions of Ace and Dmf required heating at 60°C to ensure complete dissolution. Complete dissolution was indicated by the presence of a clear solution.

The solutions were all subjected to spinning prior to beginning the main experiments to determine spinnability when using differing solvents. All solvents except Ace were able to form fibres in the test run, so

Table 1
Physical properties of the solvents investigated in this work. Values in last column calculated using reference [37].

Solvent	Boiling Point (°C)	Density (kg/m^3)	Surface Tension (mN/m)	Dielectric Constant (μS/m)	Viscosity (mPa s)	Vapor Pressure (kPa)	Difference in Solubility Parameter (MPa)$^{1/2}$
Ace	56.1	780	25.2	20.7	0.30	24.00	+0.4
Chl	62.1	1490	26.7	4.8	0.79	20.90	−0.5
Dcm	39.6	1330	26.5	9.1	0.42	58.40	+1.0
Dmf	152.8	950	37.1	37.0	0.80	0.35	+5.6
EtOh	78.5	790	22.1	24.5	1.08	5.90	+7.3
MeOh	64.6	790	22.7	32.6	0.54	13.02	+10.6
Thf	66.0	890	26.4	7.5	0.53	19.34	−0.6
Tol	110.6	870	28.5	2.4	0.56	3.79	−0.7

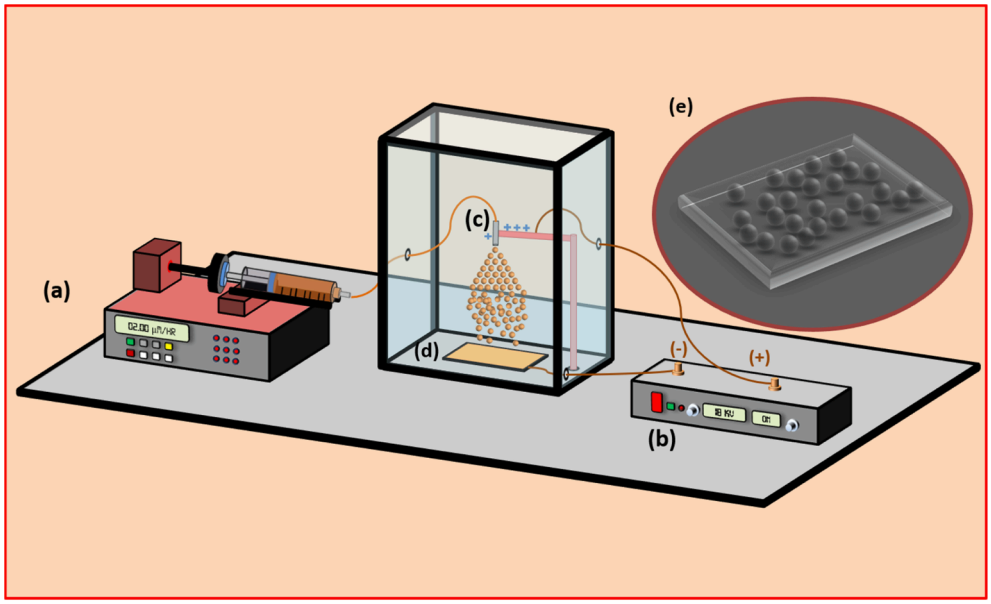

Fig. 1. A schematic representation of the electrospraying setup used: (a) solution pump, (b) high voltage power supply, (c) stainless-steel nozzle, (d) grounded collector, and (e) an insert showing a mock three-dimensional model of PCL particles produced.

Ace was excluded from the solvents investigated from this point onwards.

The spinning process was carried out with a pressurised gyration laboratory setup. This involved a small aluminium cylindrical vessel measuring 60 mm in diameter which had 24 small 0.5 mm drilled holes through its wall, in which a polymer solution was kept. The vessel was connected to a nitrogen gas supply and also a high-speed motor. Fig. 2 shows a diagrammatic representation of the setup. For these experiments, rotation speed was kept constant at 36000 rpm in order to observe differences owing to solvent and gas pressure only. The gas pressure was then varied from 0 to 0.3 MPa in 0.1 MPa increments. All experiments were carried out for 15 s using 2 mL of polymer solution

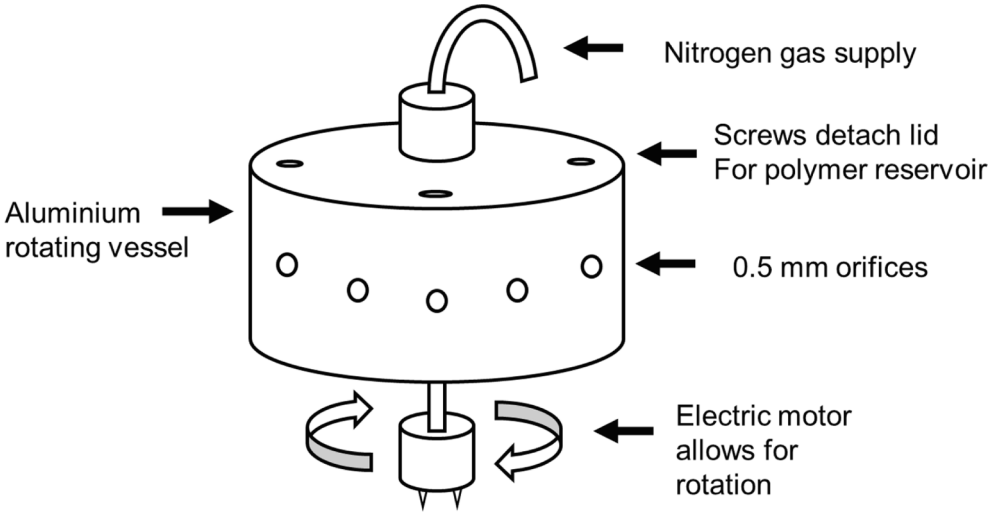

Fig. 2. Experimental setup used for the pressurised gyration process.

under ambient conditions (20–22°C) with a relative humidity range of 41–46%.

2.4. Characterisation

2.4.1. Physical observations

Electrical conductivity, surface tension, and viscosity of all solutions were measured using properly calibrated equipment.

Electrical conductivity of the electrosprayed solutions was analysed using a conductivity probe (JENWAY 3540 Conductivity Meter, Cole-Palmer, USA).

Viscosity of the electrosprayed polymer solutions was measured using a U-tube Ostwald viscometer (VWR International, USA) at 20 °C temperature and results were calculated using **Eq. (1)**:

$$\eta_{\text{rel}} = \frac{\eta}{\eta_0} = \frac{\rho t}{\rho_0 t_0} \quad (1)$$

In the equation, the η_{rel} represents the relative viscosity which is the equivalent ratio of the sample viscosity (η) divided by the viscosity of deionised water (η_0). Sample viscosity (η) is calculated using sample solution density (ρ), amount of time required for outflow of the sample solution (t), density (ρ_0), and time of outflow (t_0) for the deionised water.

Viscosity of the gyrospun polymer solutions was measured using a programmable rheometer (DV-III Ultra, Brookfield Engineering Laboratories INC, Massachusetts, USA), readings were taken at a shear stress of ≈ 5 Pa.

Surface tension of the solutions was characterised via a tensiometer (Tensiometer K9, Kruss GmbH, Germany).

For each test, all samples were investigated five times individually and standard deviations were calculated.

2.4.2. Morphological observations

Surface morphology of the PCL particles and fibres was investigated using a Scanning Electron Microscope (SEM, Hitachi S-3400n). Prior to the imaging the produced samples were gold sputter-coated (Q150R ES, Quorum Technologies); particles for 60 s and fibres for 3 min. Fibre diameters were measured using computer-aided image visualization software (Image J). Additionally, maximum, minimum, average, and standard deviation values of the obtained data were statistically estimated for each sample, and particle and fibre diameter size frequency graphs were prepared using a statistics software (Origin Pro).

3. Results and discussion

3.1. Particle production

Electrospraying is characterised as one of the most successful ways to obtain particles for various applications due to its controllable nature, and PCL is an attractive polymer to be used in conjunction with this technology due to its numerous beneficial properties such as biodegradability, biocompatibility, and non-toxic properties [38,39]. Moreover, electrosprayed PCL always finds a place in a diverse range of applications, such as tissue engineering, controlled release of active ingredients, and drug delivery applications in both micro- and nanosized diameters, while providing advanced material characteristics and high success rates in their related applications [40–42]. Manufacturing parameters are important in controlling these properties and tailoring them to intended application area. Among others, physical properties of solutions are one of the most crucial parameters and play a key role in understanding the particle morphology. Table 2 shows the viscosity, surface tension, and electrical conductivity of the binary solvent systems used to produce the microparticles in this work. Chl was chosen as a constant base solvent since it shows excellent solubility for PCL [43]. However, its low dielectric constant makes it unfavourable for fine particle production and it requires to be blended with other solvents with better dielectric constant values. Therefore, good, poor, and partially dissolving organic solvents of PCL were individually combined with Chl to analyse how they would affect the stability of the Taylor Cone, morphology of the microparticles, and alteration the microparticle size distribution. Balancing the evaporation rate, solubility, and above-mentioned characteristics of the solvents are expected to be beneficial in demonstrating how the results will differ.

Table 2
Solution properties of the binary solvents used to produce electrosprayed PCL microparticles.

Solution Content	Ratio	Viscosity (mPa s)	Surface Tension (mN/m)	Electrical Conductivity (μs/m)
Chl:MeOh	3:1	1310 ± 12	27.7 ± 0.6	4.7 ± 0.8
Chl:MeOh	1:1	1420 ± 54	26.4 ± 0.7	6.7 ± 0.3
Chl:MeOh	1:3	1490 ± 21	25.2 ± 0.3	11.0 ± 0.6
Chl:EtOh	3:1	1410 ± 32	26.6 ± 0.8	0.3 ± 0.0
Chl:EtOh	1:1	1470 ± 43	25.2 ± 0.7	0.9 ± 0.0
Chl:EtOh	1:3	1580 ± 32	24.8 ± 0.6	1.2 ± 0.0
Chl:Ace	3:1	1330 ± 24	27.8 ± 0.8	0.2 ± 0.0
Chl:Ace	1:1	1290 ± 12	27.3 ± 0.5	0.7 ± 0.0
Chl:Ace	1:3	1210 ± 45	26.6 ± 0.4	1.0 ± 0.1
Chl:Dcm	3:1	1320 ± 27	29.6 ± 0.8	0.01*
Chl:Dcm	1:1	1270 ± 72	28.3 ± 0.6	0.02*
Chl:Dcm	1:3	1190 ± 52	27.6 ± 0.3	0.04*

* Precision of the equipment was not enough to calculate the standard deviation.

The type of solvent and the ratio within the binary solutions used to dissolve PCL had the maximum influence on the physical properties of the solutions, as reflected by the differences in surface tension, viscosity, and electrical conductivity of each solution. As can be seen in Table 2, the viscosity of the samples varied between 1190 and 1580 mPa s, while the surface tension resulted in the range of 24.8 to 29.6 mN/m for electrosprayed solutions. This narrow range can be related to using the same amount of polymer concentration in each sample and minor differences correspond to the pure solvent properties given in Table 1. An increase in the viscosity and surface tension of the pure solvents was observed with each solvent combination compared to the binary systems. This additional surface tension and viscosity is believed to be provided by polymer chain entanglement, which is expected to increase the surface tension and viscosity of a polymeric solution [44]. On the contrary, even though not much difference was measured between the samples in terms of viscosity and surface tension, the electrical conductivity of the solutions varied as each solution has different dielectric constant [45].

Microparticles were obtained for each sample type (Fig. 3**)**, and they all displayed smooth and spherical characteristics, neither showing any transition to semi-spherical particles due to deformation caused by lack of evaporation, nor exhibiting hollow, irregular shaped or porous particles related to the excessive evaporation rate [46]. Therefore, it can be concluded that combinations of Chl with MeOh (Fig. 3**(a-c)**), EtOh (Fig. 3**(d-f)**), Ace (Fig. 3**(g-i)**), and Dcm (Fig. 3**(j-l)**), at different concentration levels (3:1, 1:1, and 1:3) have sufficient evaporation rate for any combination and thus smooth particle deposition occurred in electrospraying, where obtaining spherical particles was a major goal.

Fig. 4 displays the statistical data and curves of the microparticle frequency range distribution of each binary solvent system used in this study. The finest average particle diameter size was obtained where the binary system consisted of MeOh as a variable and ranged from 1.59 ± 0.36 μm (3:1 Chl:MeOh) to 1.17 ± 0.23 μm (1:3 Chl:MeOh) (Fig. 4**(a-c)**). That can be related to the fact that more conductive solutions allow further stretching to the jet during the electrohydrodynamic process, eventually reducing the diameter of the final products [47]. This was followed by EtOh, which resulted in an average particle diameter of 1.31 ± 0.35 μm (Fig. 4**(f)**), where its concentration in the binary system was higher than that of Chl (1:3 Chl:EtOh). Using the same ratio of the solvents slightly increased the average particle diameters to 1.33 ± 0.32 μm (1:1 Chl:EtOh, Fig. 4**(e)**) and finally, average particle size was pushed up to 1.43 ± 0.25 μm in where the Chl ratio exceeds the EtOh (3:1 Chl:EtOh, Fig. 4**(d)**). It was also noted that the particle size

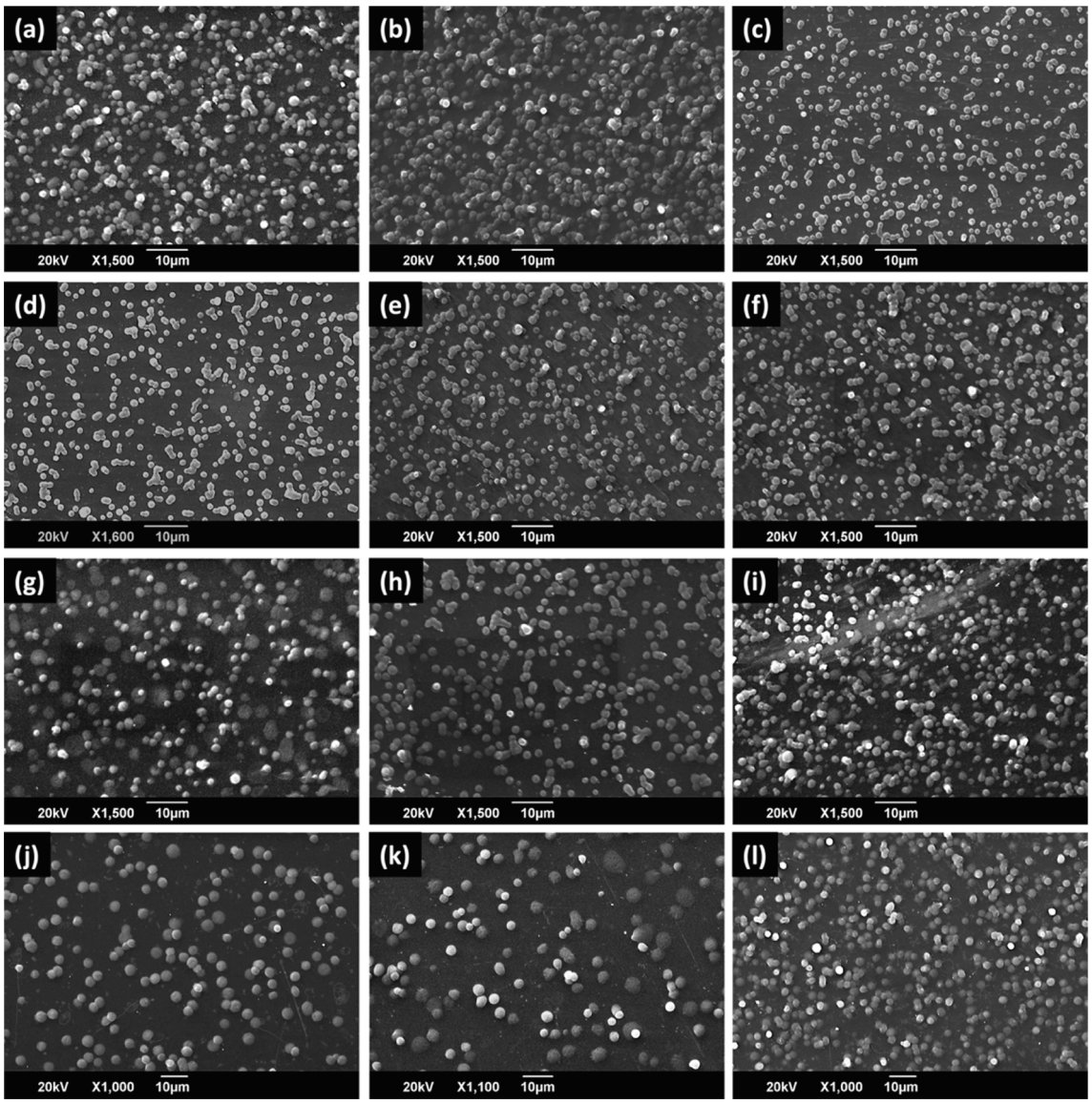

Fig. 3. SEM images of the PCL microparticles made using electrospraying in different binary solvent groups: (a-c) Chl:MeOh (3:1, 1:1, and 1:3), (d-f) Chl:EtOh (3:1, 1:1, and 1:3), (g-i) Chl:Ace (3:1, 1:1, and 1:3), and (j-l) Chl:Dcm (3:1, 1:1, and 1:3).

frequency narrowed for this sample batch.

Binary systems having Ace as the variable showed a similar effect. Average particle diameters varied between 2.03 ± 0.63 μm (Fig. 4**(g)**) and 1.69 ± 0.29 μm (Fig. 4**(i)**), and in parallel, microparticles increased in size as the Ace ratio decreased and Chl increased. Finally, gradual reduction of Chl content in Chl:Dcm binary solvent systems resulted in a parallel decrease in microparticle size. The average particle diameter size lower bound was 3.59 ± 0.54 μm, followed by 3.31 ± 0.61 μm, and finally resulted in 2.59 ± 0.33 μm as the ratio for the components of the binary solvent system changed as 3:1, 1:1, and 1:3 (Chl:Dcm, (Fig. 4**(j-l)**), respectively. Compared to other studies using the same polymer with the same molecular weight over a wide range of polymer ratios, particle diameters were decreased using this binary system, which is also beneficial for biomedical applications [48].

As the same experimental conditions were applied throughout all experiments, the difference in electrical conductivity between the organic solvents used can be underlined as the reason for the difference in particle sizes [49]. In detail, the ability of a solution to transmit stronger electrical forces during the transition from droplet to jet makes the molecules move faster. Consequently, higher electrical forces would allow further stretching of the jet during the electrospraying process, ultimately leading to smaller particle sizes [50]. In this study, the variable solvent MeOh benefited most from this phenomenon due to its high electrical properties. PCL microparticles made from MeOh having binary solvent systems exhibited the finest particle size range, followed by EtOh, Ace, and Dcm, respectively, as the particle sizes increased.

3.2. *Fibre production*

The five lone solvents used in the fibre spinning of this investigation demonstrated good solubility for PCL at 15% (w/v), except for Dmf which required heating at 60°C for complete dissolution in addition to mechanical mixing. The Hildebrand solubility parameter (δ) estimates the extent of interaction between a solvent and a solute, the closer the values are, the more likely that the two materials are miscible [51]. From the solubility parameter differences between PCL and the solvents in Table 1, it can be seen that Dmf had the highest deviation from the polymer solubility parameter, it is therefore expected that this solvent requires stimulant (heat) to increase the molecular interactions via increased kinetic energy [52].

It is important to know the differences in the properties of solvents, as they will also affect the properties of the dissolved polymer solution.

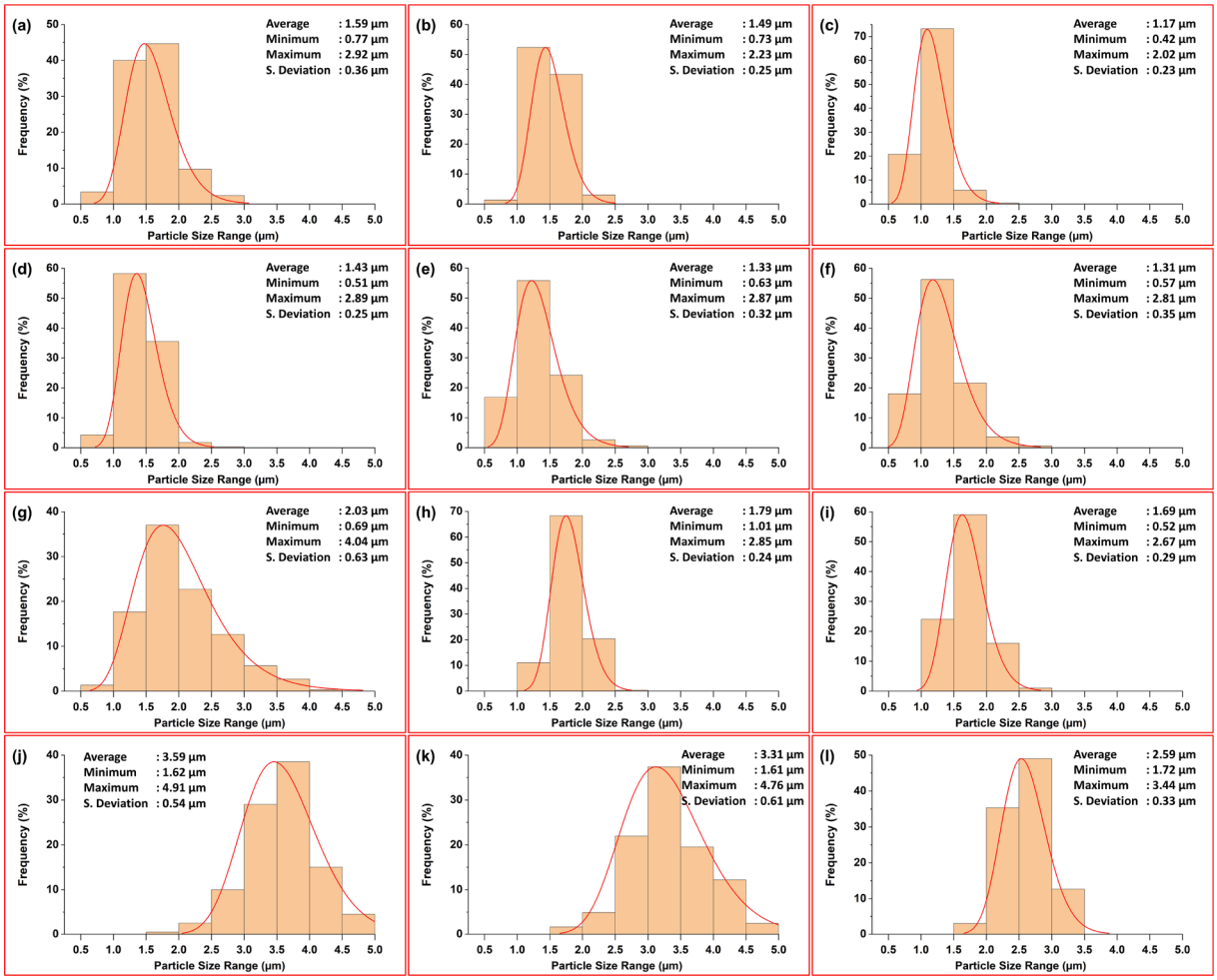

Fig. 4. Particle size distribution curves of the PCL microparticles in different binary solvent systems: (a-c) Chl:MeOh (3:1, 1:1, and 1:3), (d-f) Chl:EtOh (3:1, 1:1, and 1:3), (g-i) Chl:Ace (3:1, 1:1, and 1:3), and (j-l) Chl:Dcm (3:1, 1:1, and 1:3). All samples were produced by electrospraying under constant experimental conditions.

Table 1 highlights the key properties referred to in this paper, Table 3 shows the experimental properties of the resulting polymer solutions. It is evident that the surface tension of the solvent directly affects the surface tension of the polymer it dissolves. However, the surface tension can increase or decrease with the mass concentration, associated with attraction of polymer molecules and the interface [53]. Dmf shows the highest surface tension in both solvent and polymer solution form. In any case, the addition of PCL caused a slight increase in the surface tension of the solutions. The differences in surface tension of the polymer solution are expected to give rise to different fibre morphologies post spinning [54,55].

Initially, the five solvent-polymer systems were spun with gyration with no external gas pressure. The resulting fibres were analysed for their morphologies owing to differences purely in the use of solvent, the micrographs are presented in Fig. 5. Fibres spun with Dmf, shown in Fig. 5**(a)** showcase a highly beaded form, interconnected by very thin fibres. The bead sizes range from 20 to 240 µm and are highly polydisperse in their size distribution. This is an extreme example of the bead-on-string morphology which according to previous literature, can be attributable to viscoelasticity and surface tension of the polymer solution [56]. Of all the solvents, Dmf had the highest surface tension which could explain its beaded nature. As all the solutions were spun at the same rotational speed, they would have the same centrifugal force acting upon them and thus a higher surface tension would hinder fibre formation and possibly give rise to a bead-on-string morphology. This notion is also supported by the product of the solvent having the second highest surface tension, Tol, shown in Fig. 5**(g)**. The dominant structures are the beads which are formed by Tol dissolved PCL ranging between 10 and 160 µm, polydisperse to a lesser extent than those of the Dmf fibres. The Tol solution has a significantly higher viscosity of 3465 mPa s compared to that of Dmf at 2523 mPa s, this higher viscosity could aid in reducing the disparity of the beads as it counteracts the high surface tension during spinning.

Dcm and Chl, shown by Fig. 5**(j)** and **(m)** both have very similar surface tension values and thus produce similar morphologies when spun. Beads are present in the micrographs but are not high in numbers as with Dmf and Tol. For these solvents, the product morphology is mostly fibres which are also aligned unidirectional overall. The alignment is due to the rotation of the gyration pot and how the fibres are collected [22]. The fibres formed from the Thf, having the lowest surface tension, are completely devoid of beads as can be seen in Fig. 5**(d)**. The results presented here strongly point towards surface tension as having a dominant effect on the formation of beads during spinning as Thf had

Table 3
Physical characteristics of polymer solutions used in this study for producing fibres with pressurised gyration.

Solvent	Surface Tension (mN/m)	Viscosity (mPa s)
Dmf	34.3 ± 0.5	2523 ± 35
Thf	25.3 ± 0.4	1887 ± 26
Tol	32.3 ± 0.6	3465 ± 39
Dcm	29.7 ± 0.4	1553 ± 38
Chl	30.3 ± 0.7	2383 ± 34
3:1 Chl:MeOh	38.8 ± 0.6	2790 ± 15

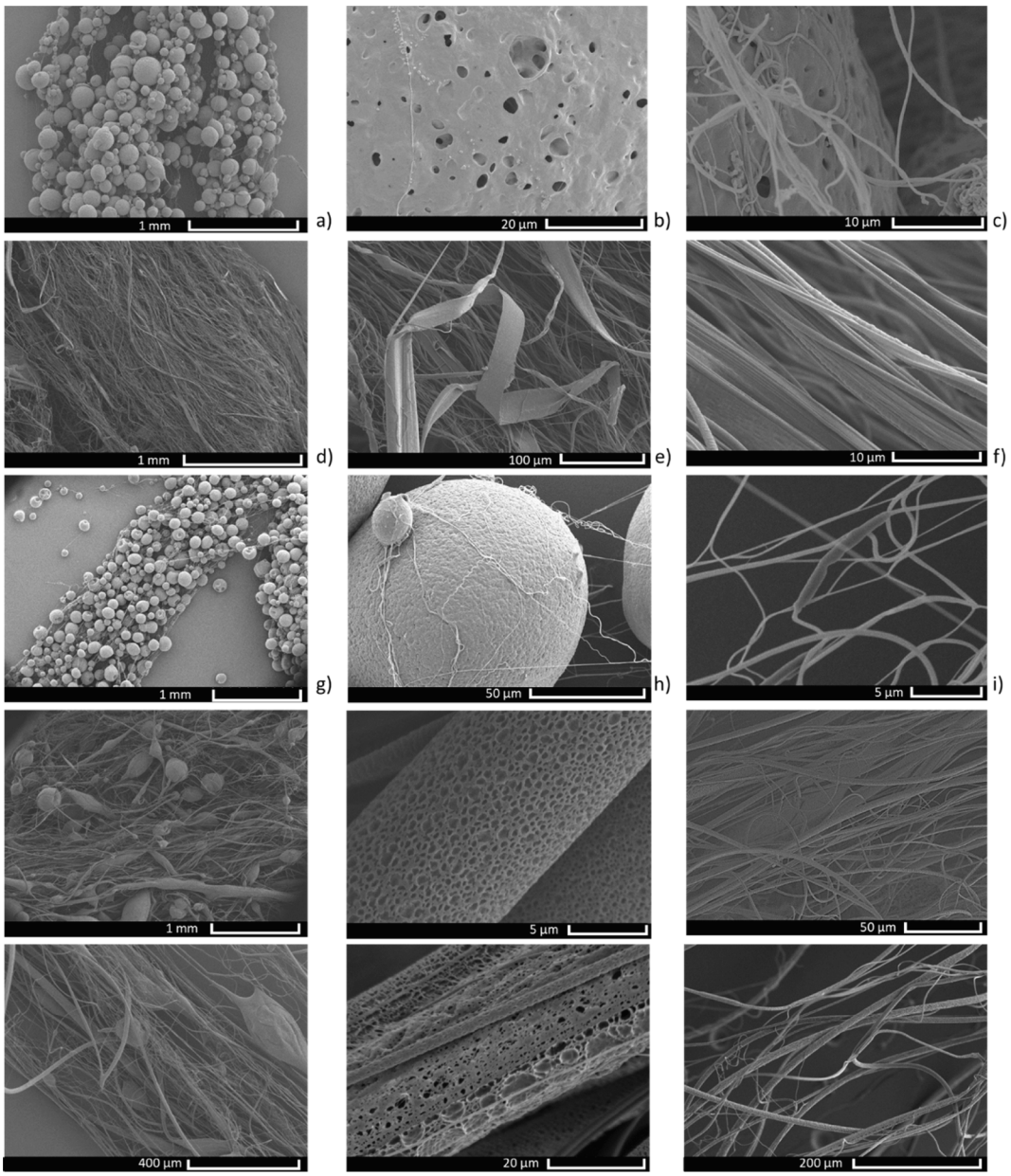

Fig. 5. SEM images of PCL fibres made using pressurised gyration in different solvents. Constituting of a macroscopic view of; (a) Dmf, (d) Thf, (g) Tol, (j) Dcm, and (m) Chl, a surface view of; (b) Dmf, (e) Thf, (h) Tol, (k) Dcm, and (n) Chl and the close-up fibre view of; (c) Dmf, (f) Thf, (i) Tol, (l) Dcm, and (o) Chl.

the lowest surface tension of all the polymer solutions.

High magnification images showing the surface of the produced fibres can be seen in Fig. 5**(b), (e), (h), (k)**, and **(n)**. Surface pores are readily found and caused by the use of highly volatile solvents which cause condensation as they evaporate, these droplets then form dimples as they too evaporate at a later stage [57]. Dcm and Chl (Fig. 5**(k)** and **(n)**) have the lowest boiling points and thus are the most volatile, and from the surface of the fibres, we can see the resulting pores. In the Dcm system, the pore sizes range from 40 to 840 nm whereas in the Chl system, the range is between 0.1 and 2.1 µm. The difference in the pore range between the two solvents is likely due to the size of the condensation droplets which are formed from the evaporation. These pores can be useful in biomedical applications where its small size can encourage cellular growth in three dimensional scaffolds [58]. Furthermore, surface pores increase the available surface area to volume ratio of the fibres which is beneficial in a multitude of applications such as drug delivery, filtration, and tissue engineering [59–62].

Looking closer at the morphology of the Tol fibres shown in Fig. 5**(h)**, it is noticed that the surface is free from porosity, instead, a slightly rough topography with small dimple-like indentations covering the bed of the beads can be seen. Having a low volatility, surface nanopores are not expected to form here. However, when observing the surface of beads formed by Dmf (Fig. 5**(b)**), craters and pores which penetrate deeper than the surface can be observed. Dmf has the highest boiling point of all the solvents tested the formation of its pores is unlikely to be attributable to condensation droplets formed by rapid evaporation. Instead, the observed pores could be the result in the solubility parameter difference which is largest in the Dmf system with a difference of 5.6 $MPa^{1/2}$ [63].

Fibres produced from Thf, which is a relatively volatile solvent, resulted in very small diameter fibres which appear to not possess a porous surface morphology as can be seen in Fig. 5**(f)**. Nonetheless, the morphology observed in Fig. 5**(e)** resembles a flat ribbon-like structure, which is not found with the use any of the other solvents tested. Ribbon-like fibres have been known to be produced in electrospinning [64–66]. This is likely due to a non-axisymmetric change in the shape of

transverse sections of the polymer jet, due to an irregularity in rotation, whilst the rapid evaporation of the solution allows shape retention after drying [67].

Upon closer magnification, we can focus on fibrous areas which were present in all the samples (Fig. 5**(c), (f), (i), (l)**, and **(o)**). Fig. 5**(c)** and **(i)** show unaligned fibres formed by Dmf and Tol, the least volatile solvents. The slow-drying nature of these solvents could be responsible for the lack of unidirectional alignment that the pressurised gyration system usually affords [68]. As the polymer jet travels through the air, it is stretched by the motion of an emerging droplet, and slower evaporation leads to a greater distance being covered by the jet. As the jet becomes thinner, the forces acting on the droplet become greater and the top of the jet becomes more unstable, causing the random alignment. Highly volatile solvents generally show an overall unidirectional alignment Fig. 6**(a)**, whilst less volatile solvents often show more random orientations Fig. 6**(b)**. Fibres produced from Thf, Dcm, and Chl (Fig. 5**(f), (l)**, and **(o)**) all show aligned morphologies which can be due to the fast-drying nature of the solvents and the unidirectional rotation of the pressurised gyration vessel.

The five solvent-polymer systems were then subjected to spinning under different gas pressures, they are summarised, and their average fibre diameters are shown in Fig. 7. Dmf systems did not show presence of fibres after 0.1 MPa of pressure. Without pressure, Dmf fibres had an average diameter of 300 ± 101 nm (Fig. 7**(a)**), at 0.1 MPa, the fibres thinned significantly to 225 ± 39 nm (Fig. 7**(b)**). The reduction in fibre diameter is the result of the external gas pressure working in tandem with the centrifugal force to extrude the polymer solution out of the orifices with a higher energy, this energy overcomes the surface tension of the polymer and causes greater thinning of the jet [69]. The resulting gas pressure also has two effects, causes alignment and reduces the bead-on-string morphology of the fibres in the Dmf systems. As discussed, due to the low volatility of Dmf, the emerging droplet from the gyration orifices thins until the initial exit energy is lost and air resistance causes random alignment. The addition of pressure allows for a higher exit velocity of the jet and thus more energy is conserved until evaporation is complete. Additionally, pressure can cause an increase in solvent volatility which causes faster drying of the jet which can aid in maintaining the extruded form of the polymer, causing more uniform fibres to be formed, as seen with Dmf fibres spun at 0.1 MPa [70]. Bead-on-string morphology is thought to be caused by axisymmetric instabilities in the production process, the application of gas is likely to have counteracted these instabilities to produce fewer beads [71].

Thf fibres had an average diameter of 515 ± 206 nm at no pressure (Fig. 7**(c)**), at 0.1 MPa, the fibres thinned to 481 ± 248 nm (Fig. 7**(d)**). This is likely due to the fact that at such a low fibre diameter (nanometre range) small variances in rotational speed from the motor can be manifested into non-uniform fibre production. Thf dissolved solution had very low viscosity and therefore will be affected by motor perturbations to a greater degree. However, beyond 0.1 MPa, the fibres began to become coarser and less uniform. This could possibly be explained by the high pressure in the small volume of the vessel causing instabilities in the jet. With volatile solvents such as Thf, the pressure can cause rapid

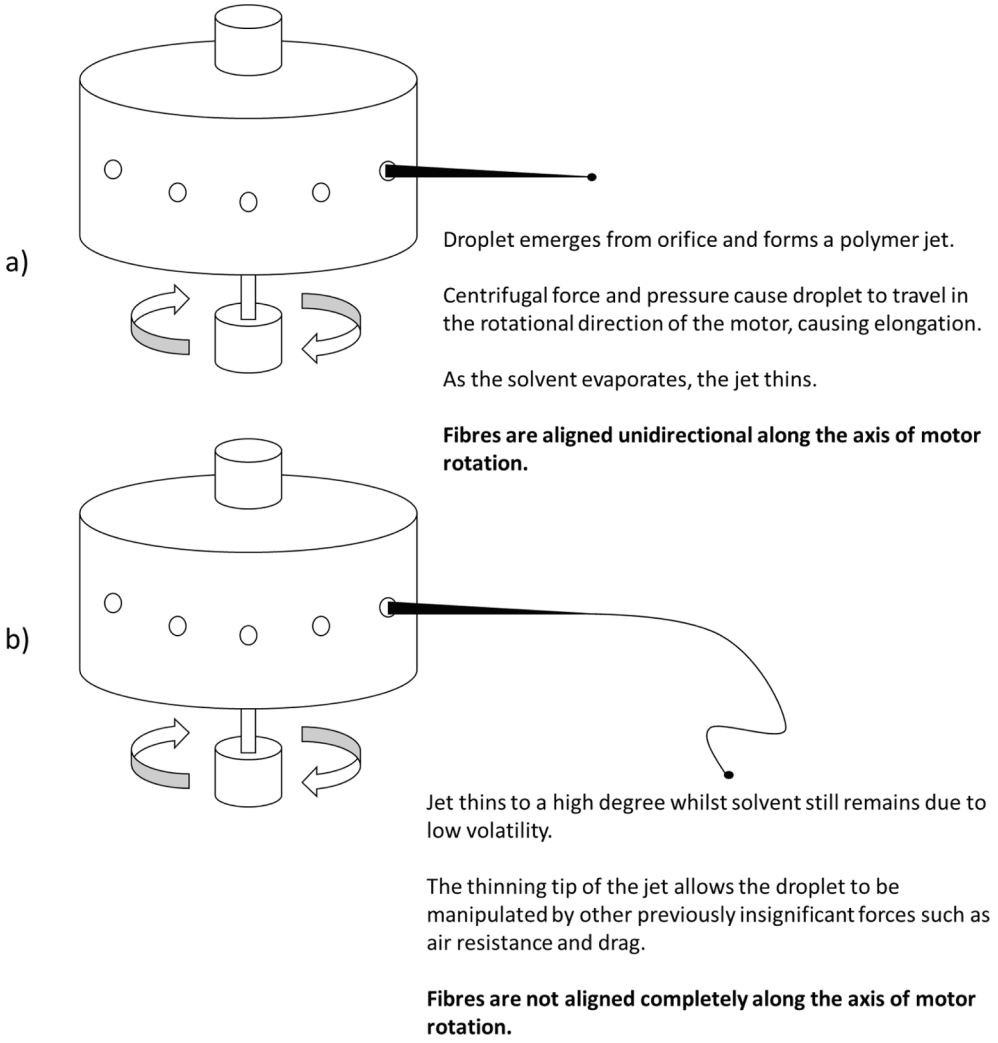

Fig. 6. Diagrammatic representation of the polymer jet when using: a) a volatile solvent, and b) a less volatile solvent.

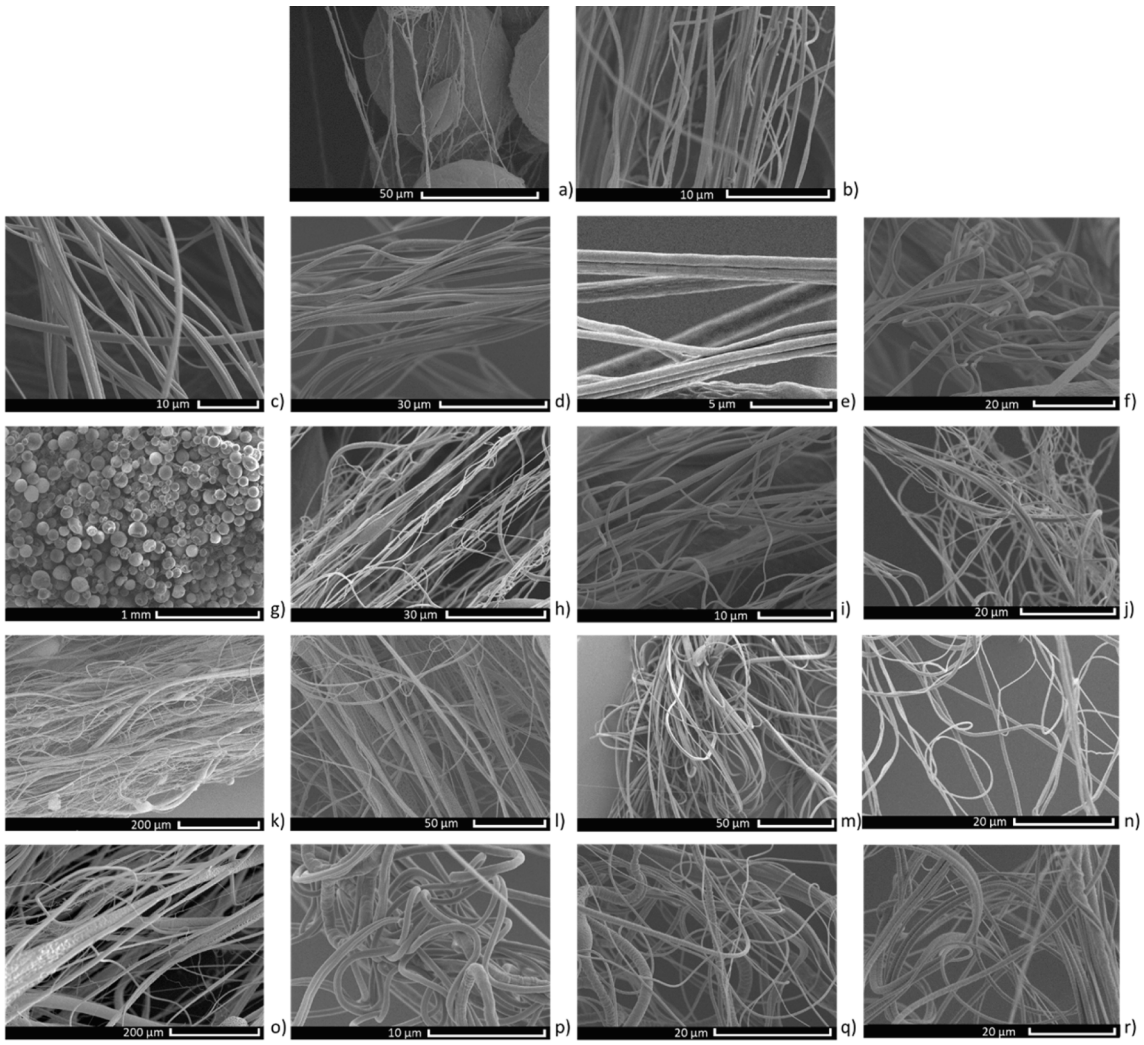

Fig. 7. SEM images of PCL fibres produced by pressurised gyration in different solvents; (a), (b) Dmf 0 MPa and 0.1 MPa pressure, (c-f) Thf 0 MPa to 0.3 MPa pressure, (g-j) Tol 0 MPa to 0.3 MPa pressure, (k-n) Dcm 0 MPa to 0.3 MPa pressure, and (o-r) Chl 0 MPa to 0.3 MPa pressure. For all instances, n = 100.

and sporadic evaporation which leads to thicker, less uniform fibres.

With Chl and Dcm, similar trends were observed. Increasing the gas pressure from 0 to 0.1 MPa causes a significant reduction in average diameter, however, further increases cause thicker fibres to be formed. Both solvents formed aligned fibres without external gas pressure, the addition of gas causes fibres to be less aligned, due to the volatile nature of the solvents and the evaporation behaviour. Tol fibres (Fig. 7 **(g)-(j)**), show a highly beaded morphology with no additional pressure, the pressure causes the beaded morphology to disappear.

Fig. 8 summarises the effect of solvent and pressure on the diameters of the investigated fibres. Firstly, it can be noticed that the solvent has a distinct effect on the resulting fibre diameters. Chl produced the thickest fibres whilst Tol produced the thinnest fibres, at no added pressure, the difference in diameter was over 25 times. Furthermore, adding pressure inside the gyration vessel caused the fibre diameters to decrease with each solvent system at 0.1 MPa. Pressure is thus a viable processing parameter that yields smaller diameter fibres compared to using no pressure at all. However, at pressures beyond 0.1 MPa, the fibre diameter increases again in all the systems, likely due to the instabilities it causes on the polymer jet. This trend is observed with all of the four solvents that could be spun at the entire pressure range. Overall, it was found that highly volatile solvents such as Chl and Dcm produced the larger diameter fibres and that the less volatile solvents were able to form much thinner fibres, this was also true at the differing levels of applied gas pressure too.

Having used the same polymer and concentration for all fibres in this study, physical properties such as surface tension and viscosity were not found to have a link to the final fibre diameter. Tol produced the thinnest fibres, but the solution also has the highest viscosity. A higher viscosity can be an indication of greater polymer chain entanglement [72,73]. Dmf has the highest surface tension but did not produce the largest diameter fibres.

3.3. Comparison of forming route

Fibres made from PCL have common occurrences in biomedical applications where a high control over end product is required and when thinner and aligned fibres benefit from a higher surface area to volume ratio [74–76]. Therefore, previously optimised 3:1, 1:1, and 1:3 Chl:MeOh binary solvents in the electrospraying work were used to dissolve PCL in order to compare and evaluate the polymeric structure production between electrospraying and pressurised gyration using the same solvent system. 15% (w/v) PCL solutions were prepared, but as PCL has poor solubility in MeOh, 1:1 and 1:3 Chl:MeOh binary solvents were not able dissolve PCL pellets fully. Therefore, experiments were carried out using only the 3:1 Chl:MeOh solvent system.

Fig. 9 illustrates the variation of morphologic features of the fibres obtained by varying the pressure applied to the PCL solution prepared with the 3:1 Chl:MeOh solvent system. Without any applied pressure, the use of 3:1 Chl:MeOh solvent system reduced the fibre diameter to

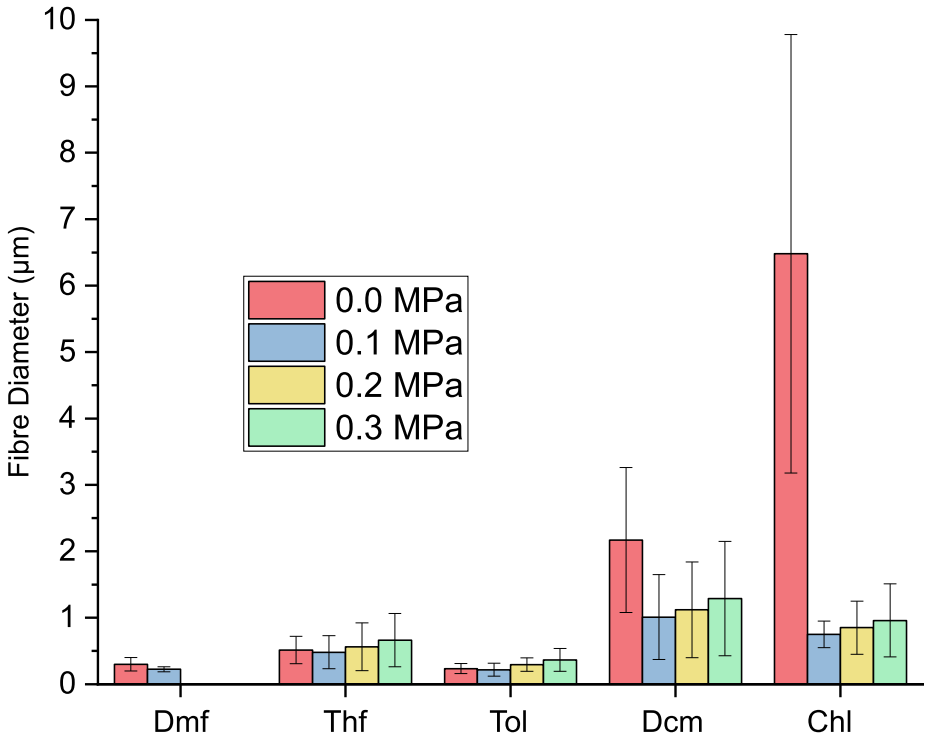

Fig. 8. Chart showing the relationship between increasing gas pressure and the resulting fibre diameters for pressurised gyration fibre production, for each case n = 100. The higher spreads of fibre diameter for Dcm (0.0 MPa) and Chl (0.0 MPa) are noted and is a characteristic of the process which benefits for the application of pressure.

4.35 ± 5.76 μm (Fig. 9 **(a)**) compared to the lone Chl solvent usage (6.48 ± 3.30 μm, Fig. 7 **(o)**) under the same experimental conditions. This phenomenon can be explained by the slightly lower volatility of MeOh than the Chl as also observed by Semiromi et al. [77]. Reduced volatility in the binary solvent system creates extended solvent evaporation, allowing more time for the fibres to stretch, resulting in smaller fibre diameters. Conversely, increased volatility can increase polymer concentration and viscosity during stretching, resulting in larger fibre diameters [78].

3:1 Chl:MeOh solvent system with applied pressures of 0.1, 0.2, and 0.3 MPa also affected the properties of PCL fibres. Fibres produced with 0.1 MPa pressure exhibited 0.78 ± 0.44 μm average diameter (Fig. 9 **(b)**) similar to the one produced with lone Chl solvent (Fig. 7 **(p)**). However, usage of binary solvent system regulated the fibre alignment and produced more aligned fibres compared to those having ribbon-like shape produced with lone Chl solvent. Reduced vaporisation time with MeOh could be responsible for this phenomenon. The average diameter further reduced to 0.67 ± 0.26 μm (Fig. 9 **(c)**) by increasing the applied pressure from 0.1 to 0.2 MPa, resulting in thinner and more unidirectional aligned and uniform fibres than the lone Chl usage displaying more stable polymer jet formation under the same experimental condition. Lastly, the average fibre diameter reduced to 0.59 ± 0.22 μm by increasing of applied pressure to 0.3 MPa (Fig. 9 **(d)**). Even though the alignment was found to be better than fibres produced with lone Chl, these fibres displayed less uniform properties than samples produced with 3:1 Chl:MeOh solvent system under 0.2 MPa pressure, likely due to the instabilities it causes on the polymer jet. Overall, solvent volatilisation was again found to be a crucial variable influencing the pressurised gyration process for the production of thinner, more aligned fibres, and uniform fibres.

However, electrospraying/electrospinning can also be applied on the larger scale with multiple needle setups and the production capability can be upscaled depending on the industrial needs [16]. Pressurised gyration, on the other hand, is newer and has found a reputable place to enable PCL fibres to be produced on an industrial scale, allowing morphology tailoring for materials produced.

4. Conclusions

The effect of various solvent systems on morphologies of electrosprayed PCL microparticles and pressure spun PCL fibres were investigated in this study. Formation mechanisms were shown to be highly dependent on production parameters, but morphological variances were found to be mainly influenced by solvent properties. For electrospraying, Chl:MeOh was found to be the best binary solvent system in terms of uniformity and particle size frequency which would fit the needs of applications at the microscale.

The effects of lone or binary solvent usage on product morphology using pressurised gyration and the effect of its gas pressure on fibre diameters have also been studied. There seems to be a link between the volatility of the solvent and the resulting fibre diameter. It was found that the surface tension of the polymer solution has an effect on bead-on-string morphology. The vapour pressure affects the surface nano pores of the fibres. Gas pressure allowed thinner fibres to be formed with this process, although high pressures can lead to thicker fibres. Gas pressure also significantly reduced the bead-on-string morphology in the polymer systems used in this work. PCL dissolved in solvents with low volatility such as Dmf and Tol showed unaligned fibres which was due to the low evaporation rate. All of the solvents differed in their solubility parameters which is likely to have had an effect on product morphology.

As the electrospraying work pointed to the Chl:MeOh binary solvent system for smaller and more uniform microparticle production, this system was also used to spin PCL fibres under different gas pressures. Enhanced fibre alignment and decreased fibre size were obtained with this binary solvent system compared to lone Chl solvent usage. Further studies can focus on using other solvents having less volatility than MeOh to form more binary solvent systems with Chl for a more detailed investigation.

The work presented here shows that PCL can successfully be produced into different polymeric structures such as particles and fibres

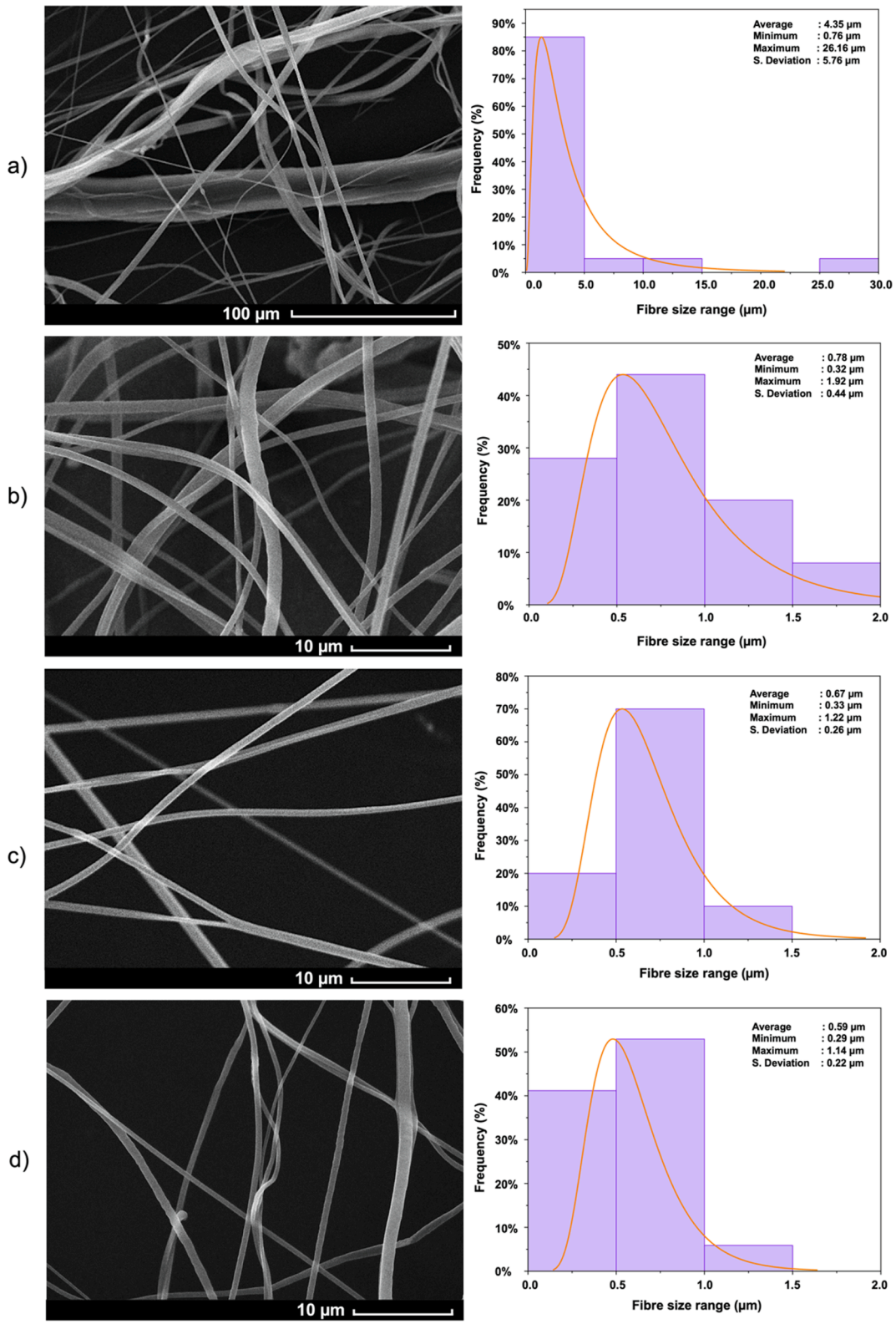

Fig. 9. SEM images of PCL fibres produced by pressurised gyration using the optimised 3:1 Chl:MeOh solvent system at different pressures; (a) 0 MPa, (b) 0.1 MPa, (c) 0.2 MPa, and (d) 0.3 MPa. For all instances, n = 100.

using both electrospraying and pressurised gyration, however the choice of solvents to dissolve PCL and the operating parameters can lead to completely different morphologies.

Data availability

The raw/processed data required to reproduce these findings cannot be shared at this time as the data also forms part of an ongoing study.

CRediT authorship contribution statement

Esra Altun: Conceptualization, Data curation, Formal analysis, Investigation, Methodology, Validation, Visualization, Writing – original draft, Writing – review & editing. **Jubair Ahmed:** Conceptualization, Data curation, Formal analysis, Investigation, Methodology, Validation, Visualization, Writing – original draft, Writing – review & editing. **Mehmet Onur Aydogdu:** Conceptualization, Data curation, Formal analysis, Investigation, Methodology, Validation, Visualization, Writing – original draft, Writing – review & editing. **Anthony Harker:** Conceptualization, Funding acquisition, Project administration, Resources, Supervision, Writing – review & editing. **Mohan Edirisinghe:** Conceptualization, Funding acquisition, Project administration, Resources, Supervision, Writing – review & editing.

Declaration of Competing Interest

The authors declare that they have no known competing financial interests or personal relationships that could have appeared to influence the work reported in this paper.

Acknowledgments

The authors wish to thank UCL Department of Archaeology and Dr Tom Gregory for the facilitation of the Scanning Electron Microscope work. We also wish to thank The Engineering and Physical Sciences Research Council UK for supporting advanced gyrospinning manufacturing work at UCL (Grants EP/L 023059/1, EP/N 034228/1 and EP/S 016872/1). Esra Altun would like to thank University College London for supporting her doctoral studies.

References

[1] B.A. Allo, A.S. Rizkalla, K. Mequanint, Synthesis and electrospinning of ε-polycaprolactone-bioactive glass hybrid biomaterials via a Sol−Gel process, Langmuir 26 (23) (2010) 18340–18348.
[2] A.G.A. Coombes, S.C. Rizzi, M. Williamson, J.E. Barralet, S. Downes, W.A. Wallace, Precipitation casting of polycaprolactone for applications in tissue engineering and drug delivery, Biomaterials 25 (2) (2004) 315–325.
[3] S. Columbus, D. Painuly, R.P. Nair, V.K. Krishnan, Role of PEGylated CdSe-ZnS quantum dots on structural and functional properties of electrospun polycaprolactone scaffolds for blood vessel tissue engineering, Eur. Polym. J. 151 (2021), 110430.
[4] I.R. Calori, G. Braga, P.D.D.C. de Jesus, H. Bi, A.C. Tedesco, Polymer scaffolds as drug delivery systems, Eur. Polym. J. 129 (2020), 109621.
[5] M.O. Aydogdu, E. Altun, J. Ahmed, O. Gunduz, M. Edirisinghe, Fiber forming capability of binary and ternary compositions in the polymer system: bacterial cellulose–polycaprolactone–polylactic Acid, Polymers 11 (7) (2019) 1148.
[6] Z. Tabia, S. Akhtach, M. Bricha, K.E. Mabrouk, Tailoring the biodegradability and bioactivity of green-electrospun polycaprolactone fibers by incorporation of bioactive glass nanoparticles for guided bone regeneration, Eur. Polym. J. 161 (2021) 110841–110853.
[7] O. Gil-Castell, J.D. Badia, A. Ribes-Greus, Tailored electrospun nanofibrous polycaprolactone/gelatin scaffolds into an acid hydrolytic solvent system, Eur. Polym. J. 101 (2018) 273–281.
[8] L. Wang, C. Wang, L. Zhou, Z. Bi, M. Shi, D. Wang, Q. Li, Fabrication of a novel Three-Dimensional porous PCL/PLA tissue engineering scaffold with high connectivity for endothelial cell migration, Eur. Polym. J. 161 (2021) 110834–110846.
[9] M.A. Woodruff, D.W. Hutmacher, The return of a forgotten polymer—Polycaprolactone in the 21st century, Prog. Polym. Sci. 35 (10) (2010) 1217–1256.
[10] S. Mahalingam, C. Bayram, M. Gultekinoglu, K. Ulubayram, S. Homer-Vanniasinkam, M. Edirisinghe, Co-Axial Gyro-Spinning of PCL/PVA/HA Core-Sheath Fibrous Scaffolds for Bone Tissue Engineering, Macromol. Biosci 2100177 (2021).
[11] M. Parhizkar, P.J.T. Reardon, J.C. Knowles, R.J. Browning, E. Stride, P.R. Barbara, A.H. Harker, M. Edirisinghe, Electrohydrodynamic encapsulation of cisplatin in poly (lactic-co-glycolic acid) nanoparticles for controlled drug delivery, Nanomedicine. Nanomed-Nanotechnol. 12 (7) (2016) 1919–1929.
[12] Y. Ziai, F. Petronella, C. Rinoldi, P. Nakielski, A. Zakrzewska, T.A. Kowalewski, W. Augustyniak, X. Li, A. Calogero, I. Sabała, B. Ding, L. De Sio, F. Pierini, Chameleon-inspired multifunctional plasmonic nanoplatforms for biosensing applications, NPG. Asia Mater. 14 (2022) 18.
[13] Y. Gao, J. Zhang, Y. Su, H. Wang, X. Wang, L. Huang, M. Yu, S. Ramakrishna, Y. Long, Recent progress and challenges in solution blow spinning, Mater. Horiz. 8 (2021) 426–446.
[14] C. Li, Y. Huang, R. Li, Y. Wang, X. Xiang, C. Zhang, D. Wang, Y. Zhou, X. Liu, W. Xu, Fabrication and properties of carboxymethyl chitosan/polyethylene oxide composite nonwoven mats by centrifugal spinning, Carbohydr. Polym. 215 (2021), 117037.
[15] R.A. Surmenev, S. Shkarina, D.S. Syromotina, E.V. Melnik, R. Shkarin, I. I. Selezneva, A.M. Ermakov, S.I. Ivlev, A. Cecilia, V. Weinhardt, T. Baumbach, T. Rijavec, A. Lapanje, M.V. Chaikina, M.A. Surmeneva, Characterization of biomimetic silicate- and strontium-containing hydroxyapatite microparticles embedded in biodegradable electrospun polycaprolactone scaffolds for bone regeneration, Eur. Polym. J. 113 (2019) 67–77.
[16] M. Parhizkar, P.J.T. Reardon, J.C. Knowles, R.J. Browning, E. Stride, R.B. Pedley, T. Grego, M. Edirisinghe, Performance of novel high throughput multi electrospray systems for forming of polymeric micro/nanoparticles, Mater. Des. 126 (2017) 73–84.
[17] E. Altun, M.O. Aydogdu, M. Crabbe-Mann, J. Ahmed, F. Brako, B. Karademir, B. Aksu, M. Sennaroglu, M.S. Eroglu, G. Ren, O. Gunduz, M. Edirisinghe, Co-Culture of Keratinocyte-*Staphylococcus aureus* on Cu-Ag-Zn/CuO and Cu-Ag-W Nanoparticle Loaded Bacterial Cellulose:PMMA Bandages, Macromol. Mater. Eng. 304 (1) (2018) 1800537.
[18] J. Ahmed, E. Altun, M.O. Aydogdu, O. Gunduz, L. Kerai, G. Ren, M. Edirisinghe, Anti-fungal bandages containing cinnamon extract, Int. Wound. J. 16 (2019) 730–736.
[19] N. Radacsi, R. Ambrus, T. Szunyogh, P. Szabó-Révész, A. Stankiewicz, A. van der Heijden, J.H. ter Horst, Electrospray crystallization for nanosized pharmaceuticals with improved properties, Cryst. Growth. Des. 12 (7) (2012) 3514–3520.
[20] S. Chakraborty, I.C. Liao, A. Adler, K.W. Leong, Electrohydrodynamics: a facile technique to fabricate drug delivery systems, Adv. Drug. Deliv. Rev. 61 (12) (2009) 1043–1054.
[21] E. Altun, M.O. Aydogdu, F. Koc, M. Crabbe-Mann, F. Brako, R. Kaur-Matharu, G. Ozen, S.E. Kuruca, U. Edirisinghe, O. Gunduz, M. Edirisinghe, Novel making of bacterial cellulose blended polymeric fiber bandages, Macromol. Mater. Eng. 303 (2018) 1700607.
[22] P.L. Heseltine, J. Ahmed, M. Edirisinghe, Developments in pressurized gyration for the mass production of polymeric fibers, Macromol. Mater. Eng. 303 (2018) 1800218.
[23] X. Hong, M. Edirisinghe, S. Mahalingam, Beads, beaded-fibres and fibres: Tailoring the morphology of poly(caprolactone) using pressurised gyration, Mater. Sci. Eng. C 69 (2016) 1373–1382.
[24] S. Mahalingam, B.T. Raimi-Abraham, D.Q.M. Craig, M. Edirisinghe, Formation of protein and protein-gold nanoparticle stabilized microbubbles by pressurized gyration, Langmuir 31 (2) (2015) 659–666.
[25] K. Nasouri, A.M. Shoushtari, A. Kaflou, Investigation of polyacrylonitrile electrospun nanofibres morphology as a function of polymer concentration, viscosity and berry number, Micro. Nano. Lett. 7 (5) (2012) 423–426.
[26] N. Obregon, V. Agubra, M. Pokhrel, H. Campos, D. Flores, D. De la Garza, Y. Mao, J. Macossay, M. Alcoutlabi, Effect of Polymer Concentration, Rotational Speed, and Solvent Mixture on Fiber Formation Using Forcespinning®, Fibers 4 (2) (2016) 20.
[27] S. Mussa Farkhani, A. Valizadeh, Electrospinning and electrospun nanofibres, IET Nanobiotechnol. 8 (2) (2014) 83–92.
[28] C.J. Thompson, G.G. Chase, A.L. Yarin, D.H. Reneker, Effects of parameters on nanofiber diameter determined from electrospinning model, Polymer 48 (23) (2007) 6913–6922.
[29] J. Ahmed, R.K. Matharu, T. Shams, U.E. Illangakoon, M. Edirisinghe, A Comparison of Electric-Field-Driven and Pressure-Driven Fiber Generation Methods for Drug Delivery, Macromol. Mater. Eng. 303 (5) (2018) 1700577.
[30] L. Wannatong, A. Sirivat, P. Supaphol, Effects of solvents on electrospun polymeric fibers: preliminary study on polystyrene, Polym. Int. 53 (11) (2004) 1851–1859.
[31] J.J. Feng, The stretching of an electrified non-Newtonian jet: A model for electrospinning, Phys. Fluids 14 (11) (2002) 3912–3926.
[32] X. Zhang, Y. Lu, Centrifugal spinning: An alternative approach to fabricate nanofibers at high speed and low cost, Polym. Rev. 54 (4) (2014) 677–701.
[33] S. Mahalingam, M. Edirisinghe, Forming of polymer nanofibers by a pressurised gyration process, Macromol. Rapid. Commun. 34 (14) (2013) 1134–1139.
[34] H. Alenezi, M.E. Cam, M. Edirisinghe, Core–sheath polymer nanofiber formation by the simultaneous application of rotation and pressure in a novel purpose-designed vessel, Appl. Phys. Rev. 8 (2021), 041412.
[35] C.J. Luo, M. Nangrejo, M. Edirisinghe, A novel method of selecting solvents for polymer electrospinning, Polymer 51 (7) (2010) 1654–1662.
[36] N. Bhardwaj, S.C. Kundu, Electrospinning: A fascinating fiber fabrication technique, Biotechnol. Adv. 28 (3) (2010) 325–347.
[37] J. Burke, Solubility parameters: theory and application, Am. Instit. Conservat. (1984).
[38] M.O. Aydogdu, J. Chou, E. Altun, N. Ekren, S. Cakmak, M. Eroglu, A.A. Osman, O. Kutlu, E.T. Oner, G. Avsar, F.N. Oktar, I. Yilmaz, O. Gunduz, Production of the biomimetic small diameter blood vessels for cardiovascular tissue engineering, Int. J. Polym. Mater. Polym. Biomater. 68 (5) (2019) 243–255.
[39] B.T. Duymaz, F.B. Erdiler, T. Alan, M.O. Aydogdu, A.T. Inan, N. Ekren, M. Uzun, Y. M. Sahin, E. Bulus, F.N. Oktar, S.S. Selvi, E. ToksoyOner, O. Kilic, M.S. Bostan, M. S. Eroglu, O. Gunduz, 3D bio-printing of levan/polycaprolactone/gelatin blends for bone tissue engineering: Characterization of the cellular behavior, Eur. Polym. J. 119 (2019) 426–437.
[40] E. Altun, M.O. Aydogdu, S.O. Togay, A.Z. Sengil, N. Ekren, M.E. Haskoylu, E. T. Oner, N.A. Altuncu, G. Ozturk, M. Crabbe-Mann, J. Ahmed, O. Gunduz,

M. Edirisinghe, Bioinspired Scaffold Induced Regeneration of Neural Tissue, Eur. Polym. J. 2019 (114) (2019) 98–108.
[41] S.K. Boda, X. Li, J. Xie, Electrospraying an enabling technology for pharmaceutical and biomedical applications: A review, J. Aerosol. Sci. 125 (2018) 164–181.
[42] J.S. Chawla, M.M. Amiji, Biodegradable poly(ε-caprolactone) nanoparticles for tumor-targeted delivery of tamoxifen, Int. J. Pharm. 249 (1) (2002) 127–138.
[43] J. Gao, S. Wu, M.A. Rogers, Harnessing Hansen solubility parameters to predict organogel formation, J. Mater. Chem. 22 (25) (2012) 12651–12658.
[44] C.J. Kuo, W.L. Lan, Gel spinning of synthetic polymer fibres. Advances in Filament Yarn Spinning of Textiles and Polymers, Woodhead Publishing, 2014.
[45] A. Castellanos, A. Pérez, Electrohydrodynamic Systems, in: C. Tropea, A.L. Yarin, J. F. Foss (Eds.), Springer Handbook of Experimental Fluid Mechanics, Berlin, Heidelberg, Springer, Berlin Heidelberg, 2007, pp. 1317–1333.
[46] Y. Gao, Y. Bai, D. Zhao, M.-W. Chang, Z. Ahmad, J.-S. Li, Tuning Microparticle Porosity during Single Needle Electrospraying Synthesis via a Non-Solvent-Based Physicochemical Approach, Polymers 7 (12) (2015) 2701–2710.
[47] X. Zong, K. Kim, D. Fang, S. Ran, B.S. Hsiao, B. Chu, Structure and process relationship of electrospun bioabsorbable nanofiber membranes, Polymer 43 (16) (2002) 4403–4412.
[48] J. Xie, J.C. Marijnissen, C.H. Wang, Microparticles developed by electrohydrodynamic atomization for the local delivery of anticancer drug to treat C6 glioma in vitro, Biomaterials 27 (17) (2006) 3321–3332.
[49] J. Xie, L.K. Lim, Y. Phua, J. Hua, C.H. Wang, Electrohydrodynamic atomization for biodegradable polymeric particle production, J. Colloid. Interface. Sci. 302 (1) (2006) 103–112.
[50] X.H. Zhong, K.S. Kim, D.F. Fang, S.F. Ran, B.S. Hsiao, B. Chu, Structure and process relationship of Electrospun bioabsorbable nanofiber membranes, Polymer 43 (2002) 4403–4412.
[51] H.J. Vandenburg, A.A. Clifford, K.D. Bartle, R.E. Carlson, J. Carroll, I.D. Newton, A simple solvent selection method for accelerated solvent extraction of additives from polymers, Analyst 124 (11) (1999) 1707–1710.
[52] S. Vyazovkin, C.A. Wight, Kinetics in solids, Annu. Rev. Phys. Chem 48 (1) (1997) 125–149.
[53] J.M. Di Meglio, R. Ober, L. Paz, C. Taupin, P. Pincus, S. Boileau, Study of the surface tension of polymer solutions: theory and experiments in theta solvent conditions, J. Phys. France 44 (9) (1983) 1035–1040.
[54] R. Casasola, N.L. Thomas, A. Trybala, S. Georgiadou, Electrospun poly lactic acid (PLA) fibres: Effect of different solvent systems on fibre morphology and diameter, Polymer 55 (18) (2014) 4728–4737.
[55] K.A.G. Katsogiannis, G.T. Vladisavljević, S. Georgiadou, Porous electrospun polycaprolactone (PCL) fibres by phase separation, Eur. Polym. J. 69 (2015) 284–295.
[56] H. Fong, I. Chun, D.H. Reneker, Beaded nanofibers formed during electrospinning, Polymer 40 (16) (1999) 4585–4592.
[57] E.U. Illangakoon, S. Mahalingam, K.R. Matharu, M. Edirisinghe, Evolution of Surface Nanopores in Pressurised Gyrospun Polymeric Microfibers, Polymers 9 (10) (2017) 508–519.
[58] Y.Z. Zhang, Y. Feng, Z.M. Huang, S. Ramakrishna, C.T. Lim, Fabrication of porous electrospun nanofibres, Nanotechnology 17 (3) (2006) 901–908.
[59] R.K. Matharu, Z. Charani, L. Ciric, U.E. Illangakoon, M. Edirisinghe, Antimicrobial activity of tellurium-loaded polymeric fiber meshes, J. Appl. Polym. Sci. 135 (25) (2018) 46368.
[60] X. Hu, S. Liu, G. Zhou, Y. Huang, Z. Xie, X. Jing, Electrospinning of polymeric nanofibers for drug delivery applications, J. Control. Release 185 (2014) 12–21.
[61] R.K. Matharu, H. Porwal, L. Ciric, M. Edirisinghe, The effect of graphene–poly (Methyl methacrylate) fibres on microbial growth, Interface. Focus 8 (3) (2018) 20170058.
[62] H.S. Yoo, T.G. Kim, T.G. Park, Surface-functionalized electrospun nanofibers for tissue engineering and drug delivery, Adv. Drug. Deliv. Rev 61 (12) (2009) 1033–1042.
[63] L. Natarajan, J. New, A. Dasari, S. Yu, M.A. Manan, Surface morphology of electrospun PLA fibers: mechanisms of pore formation, RSC Adv. 4 (83) (2014) 44082–44088.
[64] J.A. Matthews, G.E. Wnek, D.G. Simpson, G.L. Bowlin, Electrospinning of Collagen Nanofibers, Biomacromolecules 3 (2) (2002) 232–238.
[65] Z.M. Huang, Y.Z. Zhang, S. Ramakrishna, C.T. Lim, Electrospinning and mechanical characterization of gelatin nanofibers, Polymer 45 (15) (2004) 5361–5368.
[66] S. Khorshidi, A. Solouk, H. Mirzadeh, S. Mazinani, J.M. Lagaron, S. Sharifi, S. Ramakrishna, A review of key challenges of electrospun scaffolds for tissue-engineering applications, J. Tissue. Eng. Regen. Med 10 (9) (2016) 715–738.
[67] S. Koombhongse, W. Liu, D.H. Reneker, Flat polymer ribbons and other shapes by electrospinning, J. Polym. Sci. B. Polym. Phys 39 (21) (2001) 2598–2606.
[68] X. Hong, S. Mahalingam, M. Edirisinghe, Simultaneous Application of Pressure-Infusion-Gyration to Generate Polymeric Nanofibers, Macromol. Mater. Eng 302 (6) (2017) 1600564.
[69] S. Mahalingam, B.T. Raimi-Abraham, D.Q.M. Craig, M. Edirisinghe, Solubility–spinnability map and model for the preparation of fibres of polyethylene (terephthalate) using gyration and pressure, Chem. Eng. J 280 (2015) 344–353.
[70] J.P. O'Connell, J.M. Prausnitz, Thermodynamics of Gas Solubility in Mixed Solvents, Ind. Eng. Chem 3 (4) (1964) 347–351.
[71] M.J. Divvela, Y.L. Joo, Discretized modeling of beads-on-a-string morphology from electrically driven, conducting, and viscoelastic polymer jets, Int. J. Appl. Phys 121 (13) (2017), 134306.
[72] W.W. Graessley, The entanglement concept in polymer rheology. The Entanglement Concept in Polymer Rheology. Berlin, Heidelberg: Springer Berlin Heidelberg, 1974, p. 1–179.
[73] S.L. Shenoy, W.D. Bates, H.L. Frisch, G.E. Wnek, Role of chain entanglements on fiber formation during electrospinning of polymer solutions: good solvent, non-specific polymer–polymer interaction limit, Polymer 46 (10) (2005) 3372–3384.
[74] M. Chen, P.K. Patra, M.L. Lovett, D.L. Kaplan, S. Bhowmick, Role of electrospun fibre diameter and corresponding specific surface area (SSA) on cell attachment, J. Tissue. Eng. Regen. Med. 3 (4) (2009) 269–279.
[75] A.G. Guex, F.M. Kocher, G. Fortunato, E. Körner, D. Hegemann, T.P. Carrel, H. T. Tevaearai, M.N. Giraud, Fine-tuning of substrate architecture and surface chemistry promotes muscle tissue development, Acta Biomater. 8 (4) (2012) 1481–1489.
[76] V. Guarino, V. Cirillo, P. Taddei, M.A. Alvarez-Perez, L. Ambrosio, Tuning Size Scale and Crystallinity of PCL Electrospun Fibres via Solvent Permittivity to Address hMSC Response, Macromol. Biosci. 11 (12) (2011) 1694–1705.
[77] F.B. Semiromi, A. Nejaei, M. Shojaee, Effect of Methanol Concentration on the Morphology and Wettability of Electrospun Nanofibrous Membranes Based on Polycaprolactone for Oil-water Separation, Fibers Polym. 20 (2019) 2453–2460.
[78] H.M. Golecki, H. Yuan, C. Glavin, B. Potter, M.R. Badrossamay, J.A. Goss, M. D. Phillips, K.K. Parker, Effect of solvent evaporation on fiber morphology in rotary jet spinning, Langmuir 30 (44) (2014) 13369–13374.